Journal of Colloid and Interface Science 634 (2023) 963–971

Contents lists available at ScienceDirect

Journal of Colloid and Interface Science

journal homepage: www.elsevier.com/locate/jcis

Mechanical tuning of virus-like particles

Milad Radiom [a,b,*], Tim Keys [a], Yagmur Turgay [a], Ahmed Ali [a], Swapan Preet [a], Serge Chesnov [c], Viviane Lutz-Bueno [d], Emma Slack [a,*], Raffaele Mezzenga [b,*]

[a] Laboratory of Food Immunology, Institute of Food, Nutrition and Health, ETH Zürich, Zürich, Switzerland
[b] Laboratory of Food and Soft Materials, Institute of Food, Nutrition and Health, ETH Zürich, Zürich, Switzerland
[c] University of Zürich/ETH Zürich, Functional Genomics Centre Zürich, Zürich, Switzerland
[d] Paul Scherrer Institute PSI, Villigen, Switzerland

GRAPHICAL ABSTRACT

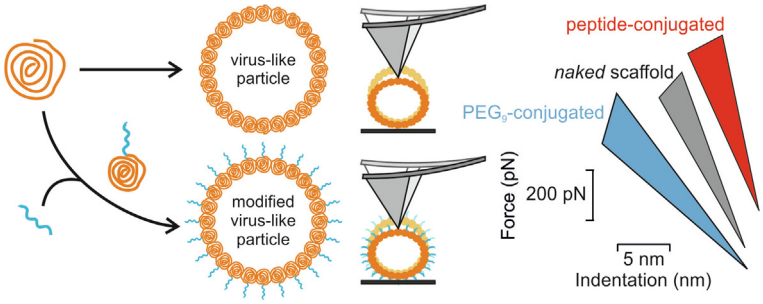

ARTICLE INFO

Article history:
Received 23 August 2022
Revised 18 December 2022
Accepted 18 December 2022
Available online 20 December 2022

Keywords:
Virus-like particle
Mucosal vaccine
Antigen conjugation
Atomic force microscopy
Nanomechanical properties
Single particle analysis

ABSTRACT

Hypothesis: Virus-like particles (VLPs) are promising scaffolds for developing mucosal vaccines. For their optimal performance, in addition to design parameters from an immunological perspective, biophysical properties may need to be considered.
Experiments: We investigated the mechanical properties of VLPs scaffolded on the coat protein of *Acinetobacter* phage AP205 using atomic force microscopy and small angle X-ray scattering.
Findings: Investigations showed that AP205 VLP is a tough nanoshell of stiffness 93 ± 23 pN/nm and elastic modulus 0.11 GPa. However, its mechanical properties are modulated by attaching muco-inert polyethylene glycol to 46 ± 10 pN/nm and 0.05 GPa. Addition of antigenic peptides derived from SARS-CoV2 spike protein by genetic fusion increased the stiffness to 146 ± 54 pN/nm although the elastic modulus remained unchanged. These results, which are interpreted in terms of shell thickness and coat protein net charge variations, demonstrate that surface conjugation can induce appreciable changes in the biophysical properties of VLP-scaffolded vaccines.
© 2022 The Author(s). Published by Elsevier Inc. This is an open access article under the CC BY license (http://creativecommons.org/licenses/by/4.0/).

1. Introduction

Vaccination via the intranasal, oral, and vaginal route is an attractive strategy for eliciting protective mucosal immune responses against pathogens that live on or enter the body via mucosal surfaces [1–3]. Efficient delivery of antigen molecules via the mucosal surfaces requires that they are delivered in particulate form, for example carried by virus-like particles (VLPs) [4].

* Corresponding authors at: Laboratory of Food Immunology, Institute of Food, Nutrition and Health, ETH Zürich, Zürich, Switzerland (M. Radiom).
E-mail addresses: milad.radiom@hest.ethz.ch (M. Radiom), emma.slack@hest.ethz.ch (E. Slack), raffaele.mezzenga@hest.ethz.ch (R. Mezzenga).

https://doi.org/10.1016/j.jcis.2022.12.090
0021-9797/© 2022 The Author(s). Published by Elsevier Inc.
This is an open access article under the CC BY license (http://creativecommons.org/licenses/by/4.0/).

VLPs self-assemble from recombinantly expressed capsid proteins (coat protein) of viruses. They lack a replication-competent genome and are highly immunogenic vaccine scaffolds because of their structural and biochemical similarity to viruses, including size, shape, repetitive surface structure, and packaging of nucleic acids [5,6]. Vaccine antigens can be chemically or genetically fused to the exterior or interior surface of the core–shell structure. VLP vaccines are already applied via parenteral routes against viral infections [6–8], and are in development for a range of other indications [9–12]. To be effective mucosal vaccines, VLPs must survive the harsh environment of the respiratory and digestive tracts, including exposure to digestive enzymes, low pH, and continuous flow of mucus [13–15]. It is therefore anticipated that the fate of VLP vaccines on mucosal surfaces depends on their biophysical properties including mechanical stiffness, enzymatic stability, and muco-adhesive properties.

A complex relationship between biophysical properties (mainly biomechanics) and biological function has been demonstrated for some viruses. For example, the capsids of *Bacillus subtilis* phage ∅29 and *Escherichia coli* phage λ were shown to sustain high internal pressures from double-stranded (ds) DNA confinement in close-to-crystalline state [16–21]. Moreover, stiffness was shown to vary with maturation of some viruses. For murine leukemia virus and human immunodeficiency virus (HIV), attenuation in stiffness was correlated with efficient host cell entry of the mature virus [22,23]. For human adenovirus, enhancement in stiffness was related to changes in the single-stranded (ss) DNA condensation state [24]. Furthermore it was demonstrated that stiffening of Minute virus of mice via coat protein point mutation impaired its infectivity and biological fitness [25], while for human adenovirus type 5 it presented no effect [26]. For VLP vaccines, conjugation to antigen molecules or molecules abrogating interactions with mucus may modulate the mechanical properties of the particles. However the effect of conjugation on mechanics, for example, with respect to resistance to mechanical stress [27], remains uninvestigated. This consideration has been the subject of recent studies for drug delivery systems using liposomal and micellar carriers [28,29], as well as in production of viruses for cancer treatment [30]. In this study we show that adding peptides or polyethylene glycol chains to the surface of the well-investigated VLP Acinetobacter Phage 205 [31] modifies the biophysical properties of VLPs, raising the question of their functional consequences.

2. Materials and methods

2.1. Production of VLPs

AP205 VLP, SpikePep1-AP205 VLP and SpikePep2-AP205 VLP. The production method of AP205 VLP and peptide-modified AP205 VLPs was identical. The bacteriophage-derived AP205 VLP spontaneously self-assembles in bacterial cytoplasm following recombinant expression of constituent coat protein. AP205, and AP205 fused to SARS-CoV2 peptides were expressed from an inducible lacUV5 promoter [32] introduced in the pRSF-DUET-1 plasmid backbone [33]. While the unmodified AP205, used as a control or a starting material for polyethylene glycol conjugation contained only a C-terminal His-tag, the constructs for expression of SpikePep1-AP205 VLP and SpikePep2-AP205 VLP additionally encoded for two peptides derived from the SARS-CoV2 spike protein at the C-terminus: namely, a 36-amino acid peptide corresponding to two linear peptide epitopes followed by a His-tag was fused to the C terminal of the AP205 coat protein to make the coat protein of SpikePep1-AP205 VLP. This peptide was repeated in tandem resulting in addition of a 72-amino acid peptide to make the coat protein of SpikePep2-AP205 VLP. VLPs were expressed in *E. coli* BL21-Gold (DE3, Agilent) in Terrific Broth [34] supplemented with 50 μg/ml kanamycin (pharma grade, AppliChem) for plasmid maintenance. Prior to induction, cultures were grown at 37°C to an OD_{600} in the range of 0.6–0.8. Expression was induced by the addition of 1 mM isopropyl-β-D-thiogalactoside (I-8000, ultrapure, <5ppm dioxane, Biosynth), and cultures were grown for a further 16–20 h at 28°C. Cell pellets were harvested by centrifugation at 8000*g*, washed once with phosphate buffered saline (PBS, BioConcept) and stored at −20°C until further processing. Expression pellets were resuspended in 40 ml of lysis buffer (50 mM Tris pH 7.5, 150 mM NaCl, 1 mM $MgCl_2$, 0.1% Triton X-100), then supplemented with 1 mg/ml lysozyme (L6876, Merck), 5 μg/ml DNase I (10104159001, Roche), and 50 μM phenylmethylsulfonyl fluoride (AB177915, 98%, abcr). Lysis was allowed to proceed for 2 h at 37°C with gentle agitation. Lysis was completed by sonication for 5 min on ice, at low amplitude, with a 6-mm probe sonicator. Lysates were cleared by centrifugation at 20,000*g* for 30 min at 4°C. VLPs were precipitated from the cell-free extract by addition of 4 mM $NiSO_4$ and pelleted by centrifugation for 2 min at 1000*g*. The precipitated material was washed once with TBS buffer (50 mM Tris pH 7.5, 150 mM NaCl), then resuspended overnight at 4°C, with gentle rotation in 40 ml of TBS with 8 mM ethylenediaminetetraacetic acid (EDTA). Contaminating lipids were removed by triton X-114 extraction (X11, laboratory grade, Sigma-Aldrich) [35] as follows: ice cold VLPs were supplemented with 1% Triton X-114, vortexed until the detergent was completely dissolved, incubated on ice for 10 min, incubated in water bath for 10 min at 42°C, centrifuged at 20,000*g* for 10 min in a rotor preheated to 37°C, the upper VLP-containing aqueous phase was recovered. VLPs were then re-precipitated by addition of 12 mM $NiSO_4$. Precipitated material was washed once with TBS, then resuspended overnight at 4°C, with gentle rotation in 15 ml of TBS with 10 mM EDTA. Finally, VLPs were dialyzed (Spectra/Por 4. 12,000 to 14,000 MWCO, 132706, SpectrumlabsID) extensively against TBS with 0.1 mM EDTA to remove remnants of $NiSO_4$. Sequence details and plasmids are provided in **SI I**. $NiSO_4$, EDTA, Tris, NaCl and Triton X-100 were purchased from Merck as laboratory grade reagents.

PEG_9-AP205 VLP. Bis(succinimidyl) nona(ethylene glycol) (BS(PEG_9), 708.71 Da, Thermo Scientific) was dissolved in anhydrous and molecular sieves dried dimethyl sulfoxide (DMSO, Sigma-Aldrich) to a concentration of 100 mM and then added to AP205 VLP suspension at 10× molar excess to AP205 coat protein. The reaction was left for 24 h at 4°C. Then after, it was quenched by adding Tris•HCl (Trizma® base, Sigma-Aldrich, and hydrochloric acid 37%, VWR) at 20–50 mM concentration and incubating for 15 min. Unreacted nona(ethylene glycol) (PEG_9) was removed using Zeba Spin Desalting Column (ThermoFisher) with molecular weight cut-off at 7 kDa.

2.2. Atomic force microscopy (AFM)

A small volume of VLP containing solution was added to freshly cleaved highly oriented pyrolytic graphite HOPG (Ted Pella, Inc.) and incubated for 15 min. Loosely bound particles were then removed by buffer exchange. Imaging and force measurements were carried with Dimension FastScan (Bruker) using AC40 BioLever Mini (Bruker). Prior to use, the cantilevers were cleaned in a UV-ozone cleaner (Novascan). Next to VLP-coated HOPG, we placed a bare freshly cleaved HOPG or mica surface for the calibration of deflection sensitivity, spring contact using thermal method, and drive-3 amplitude sensitivity [36]. No difference was found between calibration on mica or HOPG. The deflection sensitivity was calibrated using the contact region of a force curve. Typical values were around 53 nm/V. The cantilevers had spring constants around 0.06 nN/nm with a variation of about 10% among all the

cantilevers used. After calibration, the cantilever was withdrawn and moved across to the VLP-coated HOPG. During this transport, the cantilever remained wet, and the laser spot was checked to remain on the same location after re-immersion. The values of the deflection sensitivity and spring contact were re-measured at the end of the measurements to detect any appreciable variation to these values [36]. In our measurements protocol, we tuned the speed of the approach-retraction cycles by using either a sinusoidal cantilever base motion at high frequency, 1 kHz (“PeakForce tapping”), or a triangular base motion at low frequency, in the range of 1 to 20 Hz (“Ramp mode”). Imaging was carried out in PeakForce tapping mode with frequency 1 kHz, amplitude 30 nm, and setpoint around 50 pN. Generally, images of individual particles were acquired at a scan rate of <1 Hz with 200 × 200 nm^2 scan size and resolution of 64 points per line, leading to a pixel size of 3 nm. Selected particles were then imaged several times to detect any drift in the measurements. Only when there was no drift, force measurements were performed in PeakForce tapping or Ramp mode. In PeakForce tapping, force measurements followed imaging by increasing the PeakForce setpoint to higher than 100 pN but below 400 pN and thereby force and height collection were performed simultaneously at each image pixel. In Ramp mode, force measurements followed imaging by first positioning the tip on the top of one particle and then applying indentation up to a threshold force value of 200 pN at a preset base frequency. Indented particles were imaged then after in PeakForce tapping to detect sign of degradation. Deflection versus piezo displacement is then converted to force versus tip separation using common protocols [37] written in Igor Pro (Wavemetrics). The separation is arbitrarily set to zero at the point of highest contact force (i.e., the separation is relative). Fit to the linear force versus relative separation response gives the stiffness and indentation of the particle under investigation. After indentation calculation, relative separation may be shifted by a value equal to the indentation which makes it possible to superimpose the response from many different particles. Average stiffnesses were calculated from at least duplicate independent VLP preparations and AFM measurements. In each case, a new tip was used.

2.3. Small angle X-ray scattering (SAXS)

In-house SAXS measurements. Measurement with Rigaku (Cu Kα radiation, λ = 1.54 Å, and a two-dimensional argon-filled Triton detector) were performed using the following conditions: the scattering vector was calibrated and centered using silver behenate. The active range q = 0.014–0.200 $Å^{-1}$ was probed. Quartz capillaries with diameter of 1.5 mm were filled with the samples and placed onto a stainless-steel holder. The samples were measured for 4 h. The spectra are presented after background subtraction. *Synchrotron SAXS measurements*. These measurements were performed at the Swiss Light Source, cSAXS, Paul Scherrer Institute, at a wavelength of 1 Å and detector distance of 7.1065 m. The X-ray beam was focused on the detector to 50 × 25 $μm^2$ onto borosilicate glass capillaries with a 1.5-mm diameter. Ten positions were measured along the capillary with exposure times of 0.1 s followed by a pause of 0.1 s. These patterns were monitored for radiation damage and finally averaged to improve the statistics. The measurement was corrected by transmission and sample thickness. Fitting to scattering data with core–shell model was performed using SasView 4.2.2 [38].

2.4. Electrospray ionization mass spectrometry (ESI-MS)

ESI-MS data were acquired on a Synapt G2-Si quadrupole time-of-flight spectrometer (Waters, UK) with a capillary voltage of 3 V, a cone voltage of 50 V and a source temperature of 100°C. Prior to ESI-MS analysis, purified VLPs at a concentration of 1 mg/ml were reduced by dithiothreitol (DTT) at a final concentration of 50 mM. The reduction was performed for 1 h at room temperature and at pH 8. The samples were acidified with 1% formic acid (Thermo, USA), desalted using C_4 Zip Tips (Millipore, USA) and analyzed in methanol:2-propanol:0.2 % formic acid (30:20:50). The solutions were infused through a fused silica capillary (ID 75 μm) at a flow rate of 1 μl/min and sprayed through Pico Tips (ID 30 μm). The last were obtained from New Objective (Woburn, MA, USA). Recorded *m*/*z* data were deconvoluted using the MaxEnt1 software with a resolution of the output mass of 0.5 Da per channel and a Uniform Gaussian Damage Model at the half-height of 0.5 Da.

2.5. Dynamic light scattering (DLS)

DLS measurements were performed at a fixed angle of 173° by averaging 3 runs of 30-s long using Zetasizer Nano (Malvern Panalytical). The time correlation function of scattered intensity was analyzed by the CONTIN method.

2.6. Gel electrophoresis

Agarose gel electrophoresis. Native electrophoresis of intact VLPs was carried out in 0.8% agarose in TAE buffer (40 mM Tris, 0.1% acetic acid, 1 mM EDTA) with 0.5 μg/ml of ethidium bromide for visualization. Samples of 10 μg VLP were electrophoresed at 120 Volts for 90 min, then imaged on a UV transilluminator. *Reducing SDS-polyacrylamide gel electrophoresis (reducing SDS-PAGE).* Denaturing SDS-PAGE analysis was carried out in 13% Tricine gels according to the protocol of Schägger [39]. Samples of 3 μg of VLP were denatured and reduced in Laemmli sample buffer [40] at 95°C for 5 min prior to electrophoresis. Proteins were visualized by Coomassie staining.

3. Results

The VLP formed by the coat protein of *Acinetobacter* phage AP205 consists of 90 copies of coat protein dimers. In Fig. 1(a), we show an AP205 dimer as a zoom into the VLP schematic where the N- and C-termini of the polypeptides are marked to be located on the exterior surface [41]. This property offers a specific advantage that antigens genetically fused to the N- or C- termini of AP205 coat protein are presented on the outer surface of the AP205 VLP where they are available for recognition by the immune cells. This is not the case for other structurally-similar VLPs, such as the one formed by the coat protein of bacteriophage MS2 [41]. Surface antigen display on MS2 requires fusion into a surface-accessible loop, which greatly limits the range of possible antigens, or the antigen must be produced separately and chemically conjugated to the surface of the VLP. We investigated the biophysical properties of the “naked” AP205 VLP, AP205 VLP with genetic fusion to peptides, and AP205 VLP chemically conjugated to muco-inert polymers.

3.1. Characterization of modified VLPs

We employed gel electrophoresis and ESI-MS to confirm that the AP205 variants had the expected size and modifications, and that our preparations contained intact VLPs (**Figs. SI 2–1**, **SI 2–2,** and **SI 2–4**). DLS was then used to obtain the hydrodynamic size and polydispersity of the VLPs. The results of these measurements are presented in **Figs. SI 2–3** and **SI 2–5.**

N-hydroxysuccinimide (NHS) ester at termini of $BS(PEG)_9$ molecule can react with lysine groups and *N*-termini of AP205 coat proteins and form stable amide bonds. These bonds can form either

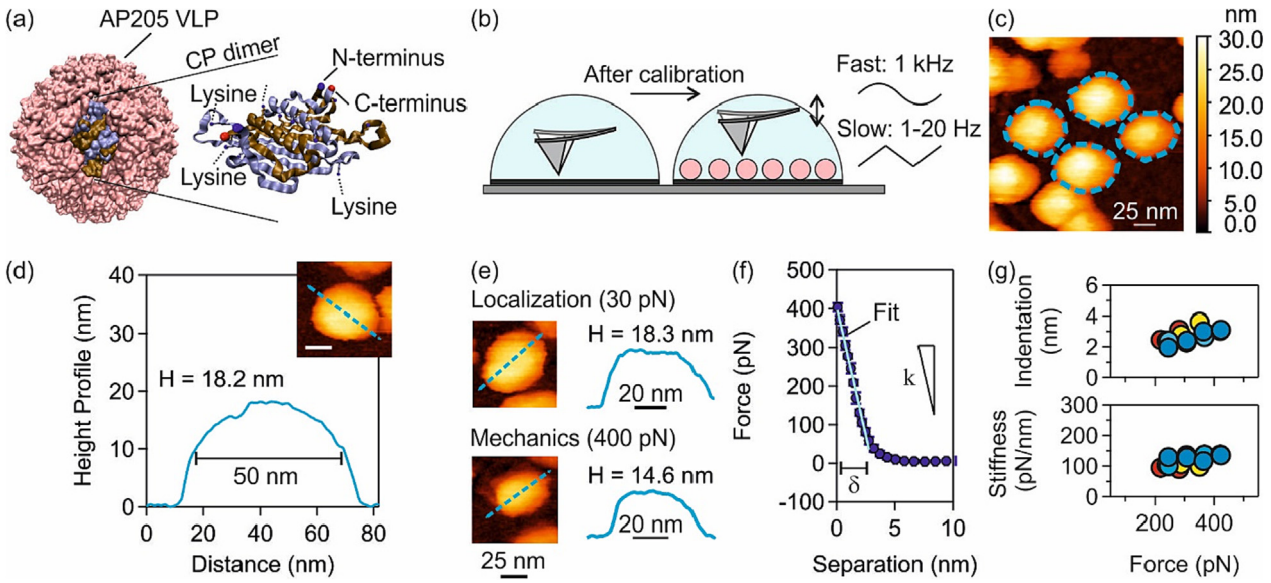

Fig. 1. (a) Schematic of AP205 VLP next to AP205 coat protein (CP) dimer [41]. The *N*-terminus (blue) of one coat protein, the C-terminus (red) of the other coat protein, and several surface lysine groups are marked. (b) Schematic of mechanical characterization by AFM of VLPs deposited on HOPG. Calibration of AFM tip was against freshly cleaved and bare HOPG or mica. The speed of approach-retraction cycle was tuned between sinusoidal cantilever base motion at high frequency (1 kHz) and triangular base motion at low frequency (1–20 Hz). (c) Several AP205 VLPs were imaged using PeakForce tapping at a low peak force setpoint of 40 pN. (d) Height profile of a single AP205 VLP (inset) giving H = 18.2 nm and AFM tip-convoluted lateral distance 50 nm. Scale bar in inset 25 nm. (e) A single AP205 VLP during localization at a peak force value of 30 pN (H = 18.3 nm) and mechanical characterization at a peak force value of 400 pN (H = 14.6 nm). (f) Average of several pixel-force curves obtained from a single AP205 VLP (same VLP as in e) at the peak force value of 400 pN resulting in stiffness (slope of the curve) k and indentation δ. (g) Indentation and stiffness measurements for several AP205 VLPs using PeakForce tapping in peak force range between 200 and 400 pN. (For interpretation of the references to colour in this figure legend, the reader is referred to the web version of this article.)

within one AP205 monomer or across two different monomers. As multiple PEG_9 linkers are bound per AP205 VLP, it is possible via this crosslinking activity to generate covalently linked AP205 coat protein dimers, trimers, and other oligomers in individual AP205 VLPs. Correspondingly, reducing SDS-PAGE demonstrated, a series of bands at molecular weights corresponding to PEG_9-AP205 coat protein dimer and trimer (**Fig. SI 2–1**). In ESI-MS spectra of PEG_9-AP205 coat proteins, focusing on masses around that of the AP205 monomer, we observed four mass peaks corresponding to one to four PEG_9 conjugated to a single AP205 coat protein (**Fig. SI 2–2**).

We then carried out agarose gel electrophoresis of the native, non-denatured VLPs. Chemical conjugation to lysine is expected to remove positive charged moieties from the surface of the VLP. In line with this, we observed an increased electrophoretic mobility (cathode (-) to anode (+)) of the fully-assembled PEG_9-AP205 VLP as compared to the unmodified AP205 VLP in the agarose gel electrophoresis (**Fig. SI 2–1**). Finally, the intensity distribution of hydrodynamic diameter of PEG_9-AP205 VLP as well as AP205 VLP were measured using DLS. We found that the hydrodynamic diameter increased from 35 ± 2 nm for AP205 VLP to 40 ± 2 nm for PEG_9-AP205 VLP with both VLPs showing a relatively monodisperse distribution (polydispersity index, PDI = 0.1) (**Fig. SI 2–3**). The slight increase in hydrodynamic diameter of PEG_9-AP205 VLP is related with the added PEG_9 coating.

Identical analyses of SpikePep1-AP205 VLP and SpikePep2-AP205 VLP were performed. The results of reducing SDS-PAGE showed a clear increase in the molecular weight of the coat protein which is in agreement with the size of the genetically added amino acid (aa) sequences (**Fig. SI 2–4**). The hydrodynamic diameters of these VLPs were 72.0 nm and 102.0 nm from DLS which show a noticeable increase as compared to AP205 VLP (**Fig. SI 2–5**). The increase is associated with the addition of the corresponding peptide sequences to AP205 coat proteins. In terms of polydispersity, both particles were found to be more polydisperse (PDI = 0.2) as compared to AP205 VLP, suggesting that the addition of peptides may slightly alter the tendency of VLPs to aggregate or self-associate.

3.2. Determination of VLP biophysical properties

AFM offers a proper spatial (< 1 nm) and force resolution (about 10 pN) for single particle investigations *in situ* and was used in virus biophysics studies such as genome contribution to stiffness [17,42,43], mutation-induced mechanical reinforcement [25,26,44] and effects from cargo filling, morphogenesis or binding of decoration proteins [45,46]. Although AFM indentation is by now a standard way of measuring the mechanical properties of viruses and VLPs, our work holds an originality in approach. Here we employed the PeakForce tapping mode of AFM. This mode applies indenting forces at much higher strain rates which makes the investigation of the viscoelastic properties of the VLPs at single particle level possible.

The AFM procedure consisted of VLP localization before and after force application (Fig. 1(b)). We used PeakForce tapping for single VLP localization at the lowest peak force values of 30–50 pN. Other localization modes, such as amplitude modulation tapping mode, were found to degrade the particles due to high forces exerted during imaging. For the purpose of mechanical characterization after localization, forces were applied using either PeakForce tapping or Ramp mode.

Images of individual "naked" AP205 VLPs in Fig. 1(c) allowed the evaluation of height distribution by placing a trace line over the image. For the VLP shown in the inset of Fig. 1(d), the trace line gave a height equal to 18.2 nm. A longer lateral dimension about 50 nm (calculated from full length at half height) is a tip convolution effect: the aspect ratio (tip height divided by its base size) results in a lateral dimension of the object that is much larger than the actual value. Tip convolution effects, artificially inflating the actual capsid size, were reported in other investigated capsid sys-

tems and imaging modes [16,22,42,45]. Hence, only height distribution provides a sound size estimation in AFM [47]. After identifying individual particles, indenting forces were applied using PeakForce tapping (or when stated, using Ramp mode). An example of the procedure is shown in Fig. 1(e, f). An individual VLP was localized with a height of 18.3 nm using a peak force value of 30 pN. The setpoint was then increased to 400 pN and we obtained simultaneously the height profile and the force curves at each image pixel. We found that the VLP height was decreased to 14.6 nm during mechanical characterization at 400 pN. One may estimate the stiffness from $k = \Delta F/\Delta H$, where F is the force, H the height, and Δ variations between high and low peak force values, and obtain 100 pN/nm for this VLP. For stiffness evaluation directly from the force curves, several pixel-force curves on top of the VLP were averaged as shown in Fig. 1(f). The force remained zero at large separations ($>$ 3 nm, relative to the point of maximum force). However, it increased after contact at lower separations. This part of the curve marks the indentation of the VLP which was found to be linear with applied force. We used the slope to calculate the stiffness, i.e., $k = dF/dx$, and the indentation $\delta = F/k$. From the fit to the curve of Fig. 1(f) we obtained a stiffness of 130 pN/nm and indentation of 3.0 nm. The difference in stiffness as obtained from the analysis of force curves or the analysis of height variation (∼23%) originates from uncertainties in each method, e.g., stiffness and deflection sensitivity in the force analysis and correct baseline determination in the height analysis. Nevertheless, we find a reasonable agreement between the two confirming the robustness of our mechanical characterization using the PeakForce tapping approach. The stiffness values were then obtained from the analysis of the force curves. In Fig. 1(g) the evolution of indentation and stiffness as a function of peak force for several AP205 VLPs are shown. In the range between 200 and 400 pN, we obtained indentation and stiffness of 2 to 4 nm and of 100 to 150 pN/nm, respectively, again in fair agreement with the analysis above.

The distribution of height for AP205 VLPs was in the range of 18.2–28.1 nm and is shown in Fig. 2(a), whereby an average height equal to 23 ± 4 nm is calculated. We additionally obtained the height distribution on large-scale, low-resolution AFM images containing many particles (**SI 3**). This data agrees well with the reported height values above. However, the high-resolution imaging approach applied throughout the manuscript allows for accurate positioning of the tip directly over the VLP, and therefore generates higher quality data for force measurements. For consistency, we therefore report only the height measurements from high-resolution imaging in the rest of the figures. The distribution of stiffness for AP205 VLPs is shown in Fig. 2(b). Stiffness varied in the range 60–130 pN/nm and an average equal to 93 ± 23 pN/nm is calculated. We used SAXS to evaluate the shell thickness of these VLPs and the scattering spectrum is shown in Fig. 2(c). Fitting the data to spherical core–shell particle resulted in (outer) diameter D = 26.3 ± 0.2 nm and shell thickness h = 3.1 ± 0.1 nm. The AFM-measured height is thereby in good agreement with the diameter measured by SAXS. We note a reduction in AFM-measured height by as much as 30% in some cases. This reduction could be attributed to adsorption-induced flatting of the VLPs but was found not to correlate with the measured stiffnesses. In **SI Note 1** we discuss the somewhat different size values obtained with DLS, SAXS and AFM. The fundamental size is closer to the SAXS value.

We then investigated the effect of chemical conjugation to muco-inert polymers on the nanomechanical properties of AP205 VLPs. As stated above, we incubated our native AP205 VLPs with BS(PEG_9), an amine-reactive homobifunctional crosslinker which added polyethylene glycol polymers to the VLP. In Fig. 3(a) an AFM image of a PEG_9-AP205 VLP is shown. The height and stiffness distribution for PEG_9-AP205 VLP are shown respectively in Fig. 3(b) and (c) and present a range of 18–30 nm and 32–60 pN/nm. The average height is calculated to be 23 ± 4 nm. The average stiffness is 46 ± 10 pN/nm and thereby a clear reduction in stiffness is observed as compared with AP205 VLP (93 ± 23 pN/nm). The SAXS spectra of PEG_9-AP205 VLP however presented no significant difference as compared to AP205 VLP as shown in Fig. 3(d). This observation together with the results of DLS, gel electrophoresis and ESI-MS (**SI 2**) indicate a dilute concentration of PEG_9 molecules on the surface of the VLP as well as possible crosslinking of individual coat proteins.

A major application of VLPs is in delivery of recombinant vaccine antigens. However, we and others have observed that particle assembly can be very sensitive to the nature of genetically fused peptides [31]. Here we investigated the effect of peptide addition to the coat protein on VLP mechanical properties. In Fig. 4(a), single particles of SpikePep1-AP205 VLP and SpikePep2-AP205 VLP were imaged. The distribution of AFM-measured height for the VLPs is shown in Fig. 4(b) and was 21.5–29.8 nm for the former and 27.4–32.7 nm the latter. Thereby we calculate an average height equal to 25 ± 3 nm and 30 ± 1 nm respectively. Similarly, the distributions of stiffness are presented in Fig. 4(c); the range was 60–140 pN/nm for the former and 62–216 pN/nm for the latter. The average stiffness is then calculated to be 100 ± 28 pN/nm and 146 ± 54 pN/nm respectively. Thereby as compared with AP205 VLP (93 ± 23 pN/nm) we found an increase in the stiffness specially in the case of SpikePep2-AP205 VLP. The SAXS spectra of SpikePep1-AP205 VLP and SpikePep2-AP205 VLP together with the spectrum of AP205 VLP are shown in Fig. 4(d). Fit of spherical core–shell particle to the spectrum of SpikePep1-AP205 VLP resulted in (outer) diameter of 27.5 ± 0.3 nm and shell thickness of 3.7 ± 0.1 nm. The significantly reduced signal to noise ratio in the case of SpikePep2-AP205 VLP is associated with its reduced colloidal stability leading to polydispersity.

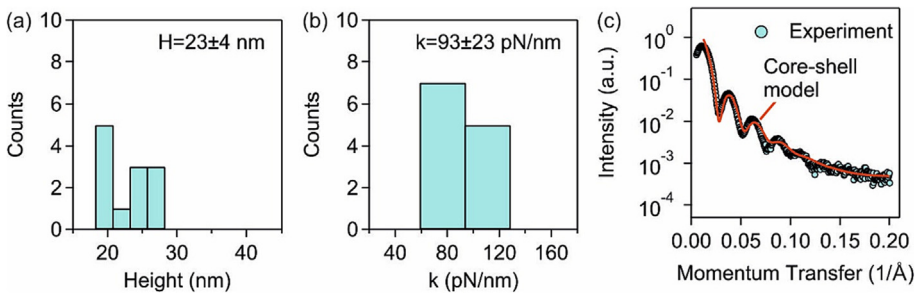

Fig. 2. Distributions of AFM-measured height (a) and stiffness (b), and SAXS spectrum (c) of AP205 VLP. Average height H = 23 ± 4 nm and stiffness k = 93 ± 23 pN/nm (number of individual AP205 VLPs n = 12). Fit to core–shell model of SAXS intensity scattering gave (outer) diameter equal to D = 26.3 ± 0.2 nm and shell thickness h = 3.1 ± 0.1 nm.

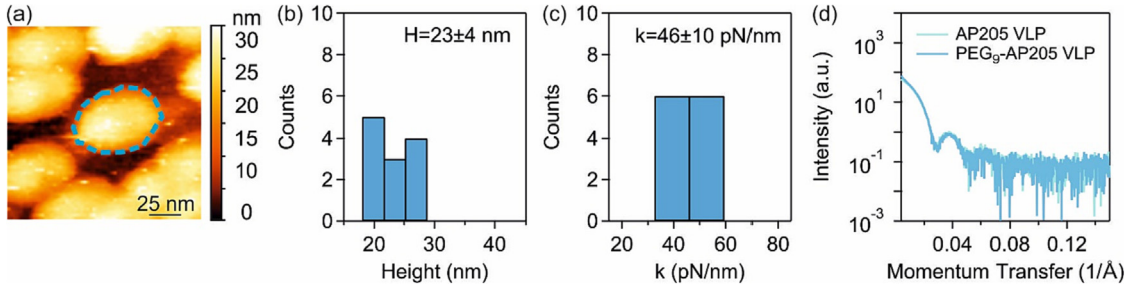

Fig. 3. (a) AFM image of PEG_9-AP205 VLPs obtained using PeakForce tapping. One VLP is marked. (b) AFM-measured height and (c) stiffness distributions of PEG_9-AP205 VLP. Average height H = 23 ± 4 nm and stiffness k = 46 ± 10 pN/nm (n = 12). (d) SAXS spectrum of PEG_9-AP205 VLP together with the spectrum of AP205 VLP.

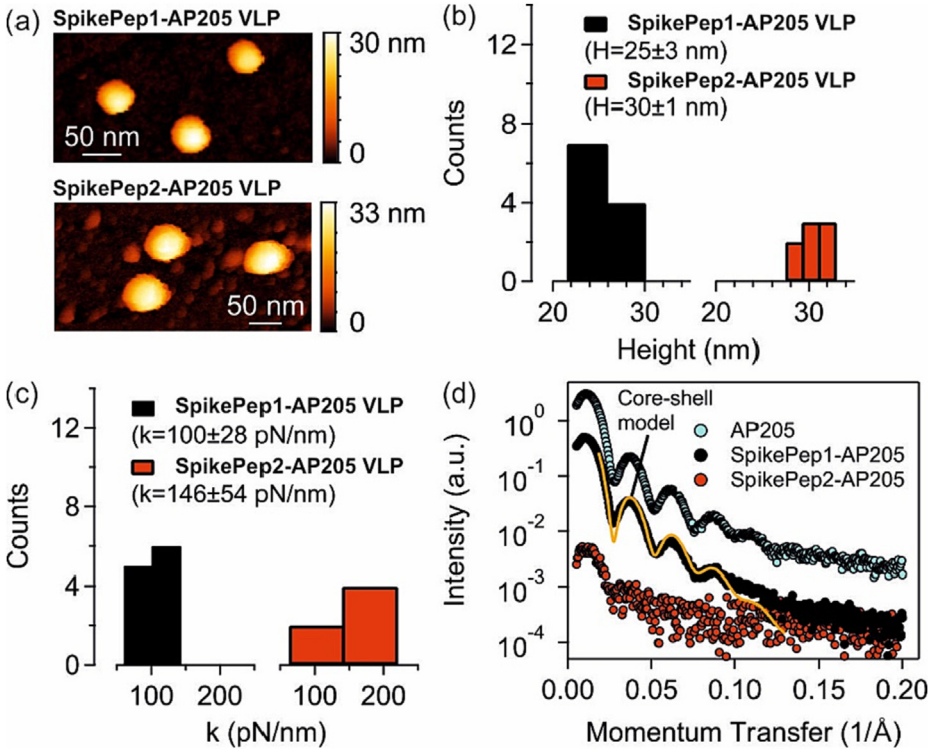

Fig. 4. (a) AFM image of SpikePep1-AP205 VLPs (top) and SpikePep2-AP205 VLPs (bottom) obtained using PeakForce tapping. (b) AFM-measured height and (c) stiffness distributions of SpikePep1-AP205 VLP and SpikePep2-AP205 VLP (n ≥ 7). (d) SAXS spectrum of SpikePep1-AP205 and SpikePep2-AP205 VLPs together with the spectrum of AP205 VLP and fit to spherical core–shell particle for SpikePep1-AP205 VLP.

4. Discussion

A stiffness–function relation (but not causation) is established for viruses such as adeno-associated viruses, rotaviruses, and HIV [23,43,48], and this relationship has been the subject of recent reviews [49,50]. However, it is not known if the biophysical properties of VLP vaccines play a role in the complex multi-step process of immune activation. On mucosal surfaces, VLPs are subject to physicochemical (ionic strength and pH) and enzymatic stress [27] and mechanical forces such as shear force during flow inside mucus constrictions or near beating cilia [51,52], or pulling force during immune activation by B cells [53,54]. If the force-induced shell deformation is not sustained by the its mechanical properties, this may lead to plastic deformation of the VLP, loss of spherical shape, or loss of uniform antigen presentation as reported in other systems [28–30] or numerically modelled [55]. Given these considerations, we speculate that properties such as size, mechanical stiffness, enzymatic stability, as well as muco-adhesive properties may be critical to eliciting an appropriate immune response. To begin our investigations in this direction, we measured the mechanical properties of several AP205 scaffolded VLPs.

The stiffness of "naked" AP205 VLP (scaffold) was found to be 93 ± 23 pN/nm. We calculated the elastic modulus for this VLP using the relation $E = Hk/2h^2$, where H is the height, k the stiffness, and h the shell thickness [56,57]. The modulus E has its origin in linear stress–strain relation first proposed by Hooke. The total energy of indentation may be divided between an out-of-plane bending energy and an in-plane compression energy. For small indentations as compared to the shell thickness the bending modulus and the stretch/compression modulus may be related to the elastic modulus E. The relative importance of the bending and stretch/compression moduli depends on the Föppl von Karman number [57]. Using the above relation we obtained $E = 0.11$ GPa for AP205 VLP. To make a comparison, the capsid of ϕ29 has an elastic modulus equal to 1.2–1.6 GPa [16], cowpea chlorotic mottle virus 0.14 GPa [44], Minute virus of mice 1.5 GPa [42], λ phage 0.2–1.0 GPa [17,18], P22 VLP 0.05 GPa [45,46], and recombinant adeno-associated virus 0.72 GPa [43] from the same relation. One notices

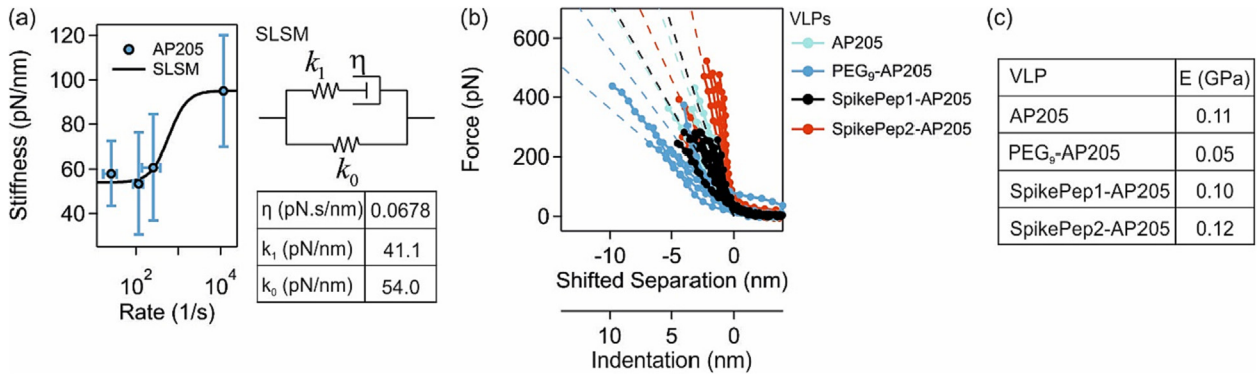

Fig. 5. (a) Stiffness at various strain rates together with fit to SLSM (**SI 5**). Schematic of the model together with panel showing the fitted parameters. (b) Superimposed force–separation (or force–indentation) curves of investigated VLPs. Broken lines in each case indicate the range of expected force responses calculated from average ± standard deviation in the stiffness values via the relation $F = k\delta$. (c) Panel summarizing the calculated elastic moduli of the investigated VLPs.

that the elastic moduli of empty capsids vary between hundreds of MPa and a few GPa, i.e., about an order of magnitude, with the AP205 VLP in the middle of this range. Due to commonality in shell thicknesses and sizes of these particles [58], the measured stiffnesses are also different within the same range (**SI 4**). This level of similarity in mechanical material properties originates from comparable intermolecular interactions between the coat proteins comprising these shells. At the level of function, however, variations of about an order of magnitude in stiffness were shown to modulate functionality; this was demonstrated in the case of murine leukemia virus and HIV [22,23].

Additional experiments showed that the full spectrum of AP205 VLP mechanics is complex. Firstly, AP205 VLPs were investigated for their viscoelastic properties (Fig. 5(a), details in **SI 5**). Using standard linear solid model (SLSM) we found a transition from stiffness k_0 = 54 pN/nm at low strain rates to stiffness $k_0 + k_1$ = 95.1 pN/nm at high rates governed by a relaxation time $\tau = \eta/k_1$ = 1.6 ms where η is the viscous term. The relaxation time is about an order of magnitude longer than the time period of tip-VLP mechanical contact during PeakForce tapping which is of the order of 0.2 ms. This difference corroborates our observation of linear force-indentation response at high strain rates (Fig. 1(g)). In **SI 6**, the yield force and indentation of the AP205 VLPs obtained in Ramp mode are reported to be 118 ± 57 pN and 3.1 ± 1.4 nm respectively. To compare with other capsids the onset of yield is much earlier with AP205 VLP, e.g. with ∅29 the yield force was in the range of 400–500 pN coinciding with the higher elastic modulus of ∅29 as compared to AP205 VLP [16]. Subsequently, when constantly imaged over a period of time, AP205 coat proteins disassembled, as shown in the image sequence of **SI 7**. This fatigue response is similar to the observations with capsids of ∅29 and λ phage [16,19].

Comparison of superimposed force–separation or force–indentation curves in Fig. 5(b) clearly shows that genetic fusion or chemical addition of molecules to AP205 VLP has an effect on the mechanical response of the particles. The stiffness of PEG_9-AP205 VLP was found to be 46 ± 10 pN/nm corresponding to an elastic modulus of E = 0.05 GPa using the previous relation. The reduction is likely related to replacement of positively-charged surface lysine and *N*-terminal groups with neutral amide bonds. The resulting attenuation in inter-coat protein electrostatic repulsion could act to reduce the force required for shell bending and compression during tip indentation [59,60]. Similarly, the stiffness of the two genetically modified VLPs, namely SpikePep1-AP205 VLP and SpikePep2-AP205 VLP, were measured to be 100 ± 28 pN/nm and 146 ± 54 pN/nm, respectively, corresponding to elastic moduli E = 0.10 GPa and E = 0.12 GPa. We thereby find that the genetic fusion of the selected aa sequences from the spike protein of SARS-Cov-2 (a short sequence of molecular weight ¼ of AP205 coat protein, and a long sequence of molecular weight ½ of AP205 coat protein) to AP205 coat protein increases the stiffness of the resulting VLP vaccine, leaving however nearly unaffected the elastic modulus. With the addition of the aa sequence of SpikePep1, a slight reduction in elastic modulus may be related with a reduction in coat protein net charge (from z ≅ + 2 to z ≅ 0), while with the aa sequence of SpikePep2, the inter-coat protein electrostatic repulsion increases again (z ≅-2) leading to a slight enhancement in the elastic modulus. The increase in stiffness may be related with an increase in shell thickness which is consistent with previous observations of stiffness enhancement when protein gpD was added to expanded λ phage and a decoration protein to expanded P22 VLP [18,19,46]. In Fig. 5(c), the panel provides a summary of the elastic moduli of the VLPs investigated in this work and in **SI 8** a summary of all the biophysical properties is provided.

In this work we showed that the addition of antigens or other molecules to AP205 VLP has an effect on its nanomechanics. In terms of immune activation, a link between biophysical properties and biological/immunological performance can be expected: these properties will affect both the resilience of the particle during delivery to secondary lymphoid tissues, and how the particle interacts with receptors on antigen presenting cells and B cells. This work suggests that the biophysical properties of VLPs can be tuned via a variety of mechanisms. This opens the door to functional experiments employing vaccination with antigenically identical, but biophysically tuned VLPs to unambiguously interrogate the link between VLP biophysics and immunogenicity.

5. Conclusion

Virus-like particles (VLPs) are highly promising, low-cost, high-productivity vaccines that are suitable not only for parenteral but also for mucosal applications [61,62]. A detailed understanding of the biophysical limits of their efficacy is crucial to the design of useful next-generation vaccines. In this work, we demonstrated that the VLP formed from recombinantly produced coat protein of *Acinetobacter* phage AP205 (AP205 VLP) is a tough nanoshell. However, the mechanical properties of this capsid are altered with the genetic fusion of peptides or chemical conjugation of polymers. This finding highlights the sensitivity of capsid structure to chemical or sequence modifications, as well as demonstrates how the biophysical properties of the capsid structure can be tuned. *In vivo* immunology experiments can now be designed using tuned, but antigenically near-identical VLPs in order to understand the funda-

mental link between VLP biophysical parameters and immunogenicity.

CRediT authorship contribution statement

Milad Radiom: Conceptulization, Data curation, Formal analysis, Funding acquisition, Methodology, Project administration, Writing - original draft, Writing - review & editing. **Tim Keys:** Data curation, Formal analysis, Methodology, Writing - review & editing. **Yagmur Turgay:** Data curation, Formal analysis, Methodology, Writing - review & editing. **Ahmed Ali:** Data curation, Formal analysis. **Swapan Preet:** Data curation, Formal analysis. **Serge Chesnov:** Data curation, Formal analysis, Methodology, Writing - review & editing. **Viviane Lütz Bueno:** Data curation, Formal analysis, Methodology, Writing - review & editing. **Emma Slack:** Conceptualization, Methodology, Writing - review & editing. **Raffaele Mezzenga:** Conceptualization, Methodology, Writing - review & editing.

Data availability

Data will be made available on request.

Declaration of Competing Interest

The authors declare that they have no known competing financial interests or personal relationships that could have appeared to influence the work reported in this paper.

Acknowledgment

M.R., Y.T., A.A. and E.S are supported by European Research Council (ERC) Grant number 865730. M.R. acknowledges the support of the Swiss National Science Foundation, Switzerland (IZSEZ0_212991) for project "Systems-level understanding of mucosal immunity using virus-like particle vaccines". E.S. acknowledges the support of the Swiss National Science Foundation, Switzerland (40B2-0_180953, 310030_185128, NCCR Microbiomes), Botnar Research Centre for Child Health Multi-investigator project "Microbiota Engineering for Child Health" and Gebert Rüf Microbials (GR073_17). We acknowledge the support of Ana Diaz and the time for SAXS measurements during proposal 20210413 granted to PSI/SLS/cSAXS.

Appendix A. Supplementary material

Supplementary data to this article can be found online at https://doi.org/10.1016/j.jcis.2022.12.090.

References

[1] E.C. Lavelle, R.W. Ward, Mucosal vaccines — fortifying the frontiers, Nat. Rev. Immunol. (2021).
[2] P.L. Ogra, H. Faden, R.C. Welliver, Vaccination strategies for mucosal immune responses, Clin. Microbiol. Rev. 14 (2) (2001) 430–445.
[3] K. Chen, A. Cerutti, Vaccination strategies to promote mucosal antibody responses, Immunity 33 (4) (2010) 479–491.
[4] N. Marasini, M. Skwarczynski, I. Toth, Oral delivery of nanoparticle-based vaccines, Expert Rev. Vaccines 13 (11) (2014) 1361–1376.
[5] N. Kushnir, S.J. Streatfield, V. Yusibov, Virus-like particles as a highly efficient vaccine platform: diversity of targets and production systems and advances in clinical development, Vaccine 31 (1) (2012) 58–83.
[6] M.O. Mohsen, L. Zha, G. Cabral-Miranda, M.F. Bachmann, Major findings and recent advances in virus–like particle (VLP)-based vaccines, Semin. Immunol. 34 (2017) 123–132.
[7] M.O. Mohsen, A.C. Gomes, M. Vogel, M.F. Bachmann, Interaction of viral capsid-derived virus-like particles (VLPs) with the innate immune system, Vaccines 6 (3) (2018) 37.
[8] H. Tariq, S. Batool, S. Asif, M. Ali, B.H. Abbasi, Virus-like particles: revolutionary platforms for developing vaccines against emerging infectious diseases, Front. Microbiol. 12 (2022).
[9] A.C. Tissot, P. Maurer, J. Nussberger, R. Sabat, T. Pfister, S. Ignatenko, H.-D. Volk, H. Stocker, P. Müller, G.T. Jennings, F. Wagner, M.F. Bachmann, Effect of immunisation against angiotensin II with CYT006-AngQb on ambulatory blood pressure: a double-blind, randomised, placebo-controlled phase IIa study, Lancet 371 (9615) (2008) 821–827.
[10] L. Zha, X. Chang, H. Zhao, M.O. Mohsen, L. Hong, Y. Zhou, H. Chen, X. Liu, J. Zhang, D. Li, K. Wu, B. Martina, J. Wang, M. Vogel, M.F. Bachmann, Development of a vaccine against SARS-CoV-2 based on the receptor-binding domain displayed on virus-like particles, Vaccines 9 (4) (2021) 395.
[11] J.G.H. Low, L.S. Lee, E.E. Ooi, K. Ethirajulu, P. Yeo, A. Matter, J.E. Connolly, D.A.G. Skibinski, P. Saudan, M. Bachmann, B.J. Hanson, Q. Lu, S. Maurer-Stroh, S. Lim, V. Novotny-Diermayr, Safety and immunogenicity of a virus-like particle pandemic influenza A (H1N1) 2009 vaccine: Results from a double-blinded, randomized Phase I clinical trial in healthy Asian volunteers, Vaccine 32 (39) (2014) 5041–5048.
[12] M.F. Bachmann, M.O. Mohsen, M.F. Kramer, M.D. Heath, Vaccination against allergy: a paradigm shift?, Trends Mol Med. 26 (4) (2020) 357–368.
[13] R.A. Cone, Barrier properties of mucus, Adv. Drug Deliv. Rev. 61 (2) (2009) 75–85.
[14] M.R. Knowles, R.C. Boucher, Mucus clearance as a primary innate defense mechanism for mammalian airways, J. Clin. Invest. 109 (5) (2002) 571–577.
[15] M.E.V. Johansson, H. Sjövall, G.C. Hansson, The gastrointestinal mucus system in health and disease, Nat. Rev. Gastroenterol. Hepatol. 10 (6) (2013) 352–361.
[16] I.L. Ivanovska, P.J.d. Pablo, B. Ibarra, G. Sgalari, F.C. MacKintosh, J.L. Carrascosa, C.F. Schmidt, G.J.L. Wuite, Bacteriophage capsids: Tough nanoshells with complex elastic properties, Proc. Natl. Acad. Sci. 101 (20) (2004) 7600–7605.
[17] I. Ivanovska, G. Wuite, B. Jönsson, A. Evilevitch, Internal DNA pressure modifies stability of WT phage, Proc. Natl. Acad. Sci. 104 (23) (2007) 9603–9608.
[18] U. Sae-Ueng, T. Liu, C.E. Catalano, J.B. Huffman, F.L. Homa, A. Evilevitch, Major capsid reinforcement by a minor protein in herpesviruses and phage, Nucleic Acids Res. 42 (14) (2014) 9096–9107.
[19] M. Hernando-Pérez, S. Lambert, E. Nakatani-Webster, C.E. Catalano, P.J. de Pablo, Cementing proteins provide extra mechanical stabilization to viral cages, Nat. Commun. 5 (1) (2014) 4520.
[20] D.E. Smith, S.J. Tans, S.B. Smith, S. Grimes, D.L. Anderson, C. Bustamante, The bacteriophage φ29 portal motor can package DNA against a large internal force, Nature 413 (6857) (2001) 748–752.
[21] A. Evilevitch, L. Lavelle, C.M. Knobler, E. Raspaud, W.M. Gelbart, Osmotic pressure inhibition of DNA ejection from phage, Proc. Natl. Acad. Sci. 100 (16) (2003) 9292–9295.
[22] N. Kol, M. Gladnikoff, D. Barlam, R.Z. Shneck, A. Rein, I. Rousso, Mechanical properties of murine leukemia virus particles: effect of maturation, Biophys. J. 91 (2) (2006) 767–774.
[23] N. Kol, Y. Shi, M. Tsvitov, D. Barlam, R.Z. Shneck, M.S. Kay, I. Rousso, A stiffness switch in human immunodeficiency virus, Biophys. J. 92 (5) (2007) 1777–1783.
[24] A. Ortega-Esteban, G.N. Condezo, A.J. Pérez-Berná, M. Chillón, S.J. Flint, D. Reguera, C. San Martín, P.J. de Pablo, Mechanics of viral chromatin reveals the pressurization of human adenovirus, ACS Nano 9 (11) (2015) 10826–10833.
[25] P.J.P. Carrillo, M. Medrano, A. Valbuena, A. Rodríguez-Huete, M. Castellanos, R. Pérez, M.G. Mateu, Amino acid side chains buried along intersubunit interfaces in a viral capsid preserve low mechanical stiffness associated with virus infectivity, ACS Nano 11 (2) (2017) 2194–2208.
[26] M.G.M. van Rosmalen, G.R. Nemerow, G.J.L. Wuite, W.H. Roos, A single point mutation in precursor protein VI doubles the mechanical strength of human adenovirus, J. Biol. Phys. 44 (2) (2018) 119–132.
[27] L.M. Ensign, R. Cone, J. Hanes, Oral drug delivery with polymeric nanoparticles: the gastrointestinal mucus barriers, Adv. Drug Deliv. Rev. 64 (6) (2012) 557–570.
[28] M.N. Holme, I.A. Fedotenko, D. Abegg, J. Althaus, L. Babel, F. Favarger, R. Reiter, R. Tanasescu, P.-L. Zaffalon, A. Ziegler, B. Müller, T. Saxer, A. Zumbuehl, Shear-stress sensitive lenticular vesicles for targeted drug delivery, Nat. Nanotechnol. 7 (8) (2012) 536–543.
[29] K.M. Takeda, Y. Yamasaki, A. Dirisala, S. Ikeda, T.A. Tockary, K. Toh, K. Osada, K. Kataoka, Effect of shear stress on structure and function of polyplex micelles from poly(ethylene glycol)-poly(l-lysine) block copolymers as systemic gene delivery carrier, Biomaterials 126 (2017) 31–38.
[30] D. Loewe, J. Häussler, T.A. Grein, H. Dieken, T. Weidner, D. Salzig, P. Czermak, Forced degradation studies to identify critical process parameters for the purification of infectious measles virus, Viruses 11 (8) (2019).
[31] A.C. Tissot, R. Renhofa, N. Schmitz, I. Cielens, E. Meijerink, V. Ose, G.T. Jennings, P. Saudan, P. Pumpens, M.F. Bachmann, Versatile virus-like particle carrier for epitope based vaccines, PLoS One 5 (3) (2010) e9809.
[32] U. Deuschle, W. Kammerer, R. Gentz, H. Bujard, Promoters of Escherichia coli: a hierarchy of in vivo strength indicates alternate structures, EMBO J. 5 (11) (1986) 2987–2994.
[33] N.H. Tolia, L. Joshua-Tor, Strategies for protein coexpression in Escherichia coli, Nat. Methods 3 (1) (2006) 55–64.
[34] Terrific Broth (TB) Medium, Cold Spring Harbor Protocols, 2015.
[35] Y. Aida, M.J. Pabst, Removal of endotoxin from protein solutions by phase separation using triton X-114, J. Immunol. Methods 132 (2) (1990) 191–195.
[36] M. Offroy, A. Razafitianamaharavo, A. Beaussart, C. Pagnout, J.F.L. Duval, Fast automated processing of AFM PeakForce curves to evaluate spatially resolved

Young modulus and stiffness of turgescent cells, RSC Adv. 10 (33) (2020) 19258–19275.
[37] H.J. Butt, B. Cappella, M. Kappl, Force measurements with the atomic force microscope: Technique, interpretation and applications, Surf. Sci. Rep. 59 (2005) 1–152.
[38] This work benefited from the use of the SasView application, originally developed under NSF award DMR-0520547. SasView contains code developed with funding from the European Union's Horizon 2020 research and innovation programme under the SINE2020 project, grant agreement No 654000.
[39] H. Schägger, Tricine–SDS-PAGE, Nat. Protoc. 1 (1) (2006) 16–22.
[40] Laemmli Sample Buffer (4×), Cold Spring Harbor Protocols, 2015.
[41] M. Shishovs, J. Rumnieks, C. Diebolder, K. Jaudzems, L.B. Andreas, J. Stanek, A. Kazaks, S. Kotelovica, I. Akopjana, G. Pintacuda, R.I. Koning, K. Tars, Structure of AP205 coat protein reveals circular permutation in ssRNA bacteriophages, J. Mol. Biol. 428 (21) (2016) 4267–4279.
[42] C. Carrasco, A. Carreira, I.A.T. Schaap, P.A. Serena, J. Gómez-Herrero, M.G. Mateu, P.J.d. Pablo, DNA-mediated anisotropic mechanical reinforcement of a virus, Proc. Natl. Acad. Sci. 103 (37) (2006) 13706–13711.
[43] C. Zeng, S. Moller-Tank, A. Asokan, B. Dragnea, Probing the link among genomic cargo, contact mechanics, and nanoindentation in recombinant adeno-associated virus 2, J. Phys. Chem. B 121 (8) (2017) 1843–1853.
[44] J.P. Michel, I.L. Ivanovska, M.M. Gibbons, W.S. Klug, C.M. Knobler, G.J.L. Wuite, C.F. Schmidt, Nanoindentation studies of full and empty viral capsids and the effects of capsid protein mutations on elasticity and strength, Proc. Natl. Acad. Sci. 103 (16) (2006) 6184–6189.
[45] A. Llauró, D. Luque, E. Edwards, B.L. Trus, J. Avera, D. Reguera, T. Douglas, P.J.d. Pablo, J.R. Castón, Cargo–shell and cargo–cargo couplings govern the mechanics of artificially loaded virus-derived cages, Nanoscale 8 (17) (2016) 9328–9336.
[46] A. Llauró, B. Schwarz, R. Koliyatt, P.J. de Pablo, T. Douglas, Tuning viral capsid nanoparticle stability with symmetrical morphogenesis, ACS Nano 10 (9) (2016) 8465–8473.
[47] B. Voigtländer, Artifacts in AFM, in: Atomic Force Microscopy, 2019, Springer, pp. 137–146.
[48] M. Jiménez-Zaragoza, M.P.L. Yubero, E. Martín-Forero, J.R. Castón, D. Reguera, D. Luque, P.J. de Pablo, J.M. Rodríguez, Biophysical properties of single rotavirus particles account for the functions of protein shells in a multilayered virus, Elife 7 (2018) e37295.
[49] R. Zandi, B. Dragnea, A. Travesset, R. Podgornik, On virus growth and form, Phys. Rep. 847 (2020) 1–102.
[50] R.F. Bruinsma, G.J.L. Wuite, W.H. Roos, Physics of viral dynamics, Nat. Rev. Phys. 3 (2) (2021) 76–91.
[51] M. Radiom, R. Hénault, S. Mani, A.G. Iankovski, X. Norel, J.-F. Berret, Magnetic wire active microrheology of human respiratory mucus, Soft Matter 17 (32) (2021) 7585–7595.
[52] M. Chioccioli, L. Feriani, J. Kotar, P.E. Bratcher, P. Cicuta, Phenotyping ciliary dynamics and coordination in response to CFTR-modulators in Cystic Fibrosis respiratory epithelial cells, Nat. Commun. 10 (1) (2019) 1763.
[53] P. Tolar, K.M. Spillane, Force generation in B-cell synapses: mechanisms coupling B-cell receptor binding to antigen internalization and affinity discrimination, Adv. Immunol. 123 (2014) 69–100.
[54] K.M. Spillane, P. Tolar, B cell antigen extraction is regulated by physical properties of antigen-presenting cells, J. Cell Biol. 216 (1) (2016) 217–230.
[55] T. Hou, Y. Ren, Y. Chan, J. Wang, Y. Yan, Flow-induced shear stress and deformation of a core–shell-structured microcapsule in a microchannel, Electrophoresis n/a (n/a).
[56] M.P. Neubauer, M. Poehlmann, A. Fery, Microcapsule mechanics: from stability to function, Adv. Colloid Interface Sci. 207 (2014) 65–80.
[57] M. Buenemann, P. Lenz, Elastic properties and mechanical stability of chiral and filled viral capsids, Phys. Rev. E 78 (5) (2008) 051924.
[58] A. Lošdorfer Božič, A. Šiber, R. Podgornik, Statistical analysis of sizes and shapes of virus capsids and their resulting elastic properties, J. Biol. Phys. 39 (2) (2013) 215–228.
[59] J. Lidmar, L. Mirny, D.R. Nelson, Virus shapes and buckling transitions in spherical shells, Phys. Rev. E 68 (5) (2003) 051910.
[60] M. Buenemann, P. Lenz, Mechanical limits of viral capsids, Proc. Natl. Acad. Sci. 104 (24) (2007) 9925–9930.
[61] J.C. Caldeira, M. Perrine, F. Pericle, F. Cavallo, Virus-like particles as an immunogenic platform for cancer vaccines, Viruses 12 (5) (2020).
[62] S. Nooraei, H. Bahrulolum, Z.S. Hoseini, C. Katalani, A. Hajizade, A.J. Easton, G. Ahmadian, Virus-like particles: preparation, immunogenicity and their roles as nanovaccines and drug nanocarriers, J. Nanobiotechnol. 19 (1) (2021) 59.